Dual-wavelength band spectroscopic optical frequency domain imaging using plasmon-resonant scattering in metallic nanoparticles

Tae Shik Kim,[1] Sun-Joo Jang,[1,2] Nuri Oh,[3] Yongjoo Kim,[1] Taejin Park,[1] Jiho Park,[3] and Wang-Yuhl Oh[1,*]

[1]*Department of Mechanical Engineering, KAIST, 335 Gwahangno, Yuseong-gu, Daejeon 305-701, South Korea*

[2]*Graduate School of Medical Science and Engineering, KAIST, 335 Gwahangno, Yuseong-gu, Daejeon 305-701, South Korea*

[3]*Department of Bio and Brain Engineering, KAIST, 335 Gwahangno, Yuseong-gu, Daejeon 305-701, South Korea*

**Corresponding author: woh1@kaist.ac.kr*

Received March 26, 2014; accepted April 11, 2014;
posted April 22, 2014 (Doc. ID 208978); published May 15, 2014

We demonstrate a dual-wavelength band optical frequency domain imaging (OFDI) system that provides high-resolution spectroscopic imaging with metallic nanoparticles as exogenous contrast agents. The local increase of the OFDI signal by elastic scattering from two different custom-fabricated nonspherical nanoparticles resonant at each wavelength band of the system was successfully detected, and we were able to distinguish and visualize the location of each of the nanoparticles in a scattering sample and in biological tissue. © 2014 Optical Society of America

OCIS codes: (110.4500) Optical coherence tomography; (240.6680) Surface plasmons; (160.4236) Nanomaterials.
http://dx.doi.org/10.1364/OL.39.003082

Spectroscopic optical coherence tomography (SOCT) enables high-resolution depth-section imaging with spectral information about a biological sample [1]. It enhances image contrast through visualization of wavelength dependent scattering/absorption properties of the biological medium or externally injected contrast agents and provides information that is complementary to standard reflectance-based optical coherence tomography (OCT) images. For example, SOCT can assess oxygen saturation levels of the blood in vessels by utilizing the fact that the absorption spectral profile of the blood varies with hemoglobin oxygen levels [2]. While endogenous contrast agents have been successfully introduced for the SOCT technique, exogenous contrast agents would also be beneficial to further enhance local spectral contrast. Since OCT is a coherent imaging technique, fluorescence, which lacks phase relation with the incident light, cannot be used as a contrast agent in OCT. Metallic nanoparticles (MNPs) have been recognized as promising exogenous contrast agents for SOCT because light is absorbed and elastically scattered at the metal/dielectric interface of the MNPs. This plasmon-induced process on MNPs drastically increases optical absorption as well as scattering at resonant wavelength, which provides excellent contrast in SOCT imaging. In addition, the plasmon-resonant wavelength of the MNPs can be tuned by engineering their shape and size.

In previous work, plasmon-resonant MNPs have been mainly utilized to increase the light absorption resulting in local optical contrast [3,4]. By comparing OCT images taken both prior to and subsequent to the injection of nanoparticles, the concentration and the location of contrast agents inside a tissue have been visualized. Demonstrations of the absorption dominant MNPs as exogenous contrast agents have shown the utility of plasmon resonance for spectroscopic contrast techniques in OCT. In this Letter, we present spectroscopic optical frequency domain imaging (OFDI), one form of the second generation OCT techniques [5,6], that utilizes plasmon-resonant scattering in MNPs. By utilizing the local increase of the OFDI signal from strong scattering rather than absorption in the MNPs at the resonant wavelength, three-dimensional spectroscopic imaging can be achieved. A novel time-domain multiplexed dual-wavelength band OFDI system that acquires images from both the 1040 and 1300 nm bands in every alternating A-line, and two different custom-fabricated MNPs with resonant wavelengths matching each wavelength band of the system, enabled us to perform high-resolution spectroscopic OFDI imaging simply by comparing images acquired at each of the wavelength bands.

Since technologies for the OFDI system and its components are mature in the 1040 and 1300 nm regions, we developed a dual-wavelength band OFDI system that generated images at these two wavelength bands as depicted in Fig. 1(a). For the light source of the system, we built a pair of short-length ring cavity wavelength swept lasers (WSL) operating at the 1040 and 1300 nm ranges [7]. The Fabry–Perot filter (Lambdaquest X1300-160-1000, H1050-140-700) inside each ring cavity was driven at the same resonant frequency with 180° phase difference to each other, as shown in Fig. 1(b). The intracavity semiconductor optical amplifiers (Thorlabs BOA1130U2, Innolume SOA-1060-100-HI-24dB) were modulated in such a way that each laser was turned on only during the positive wavelength sweeps that make each laser source operate one after the other. Isolators were located inside the cavity in order to prevent backward light amplifications. The outputs of the WSLs were combined with a dichroic mirror, which provided a time-domain multiplexed dual-wavelength band swept source. The A-line rate of the combined light source was 120 kHz, and the wavelength tuning ranges of the two WSLs were 100 and 120 nm, respectively. Since the two wavelength bands share the system interferometer, we built it using free-space optics to minimize the wavelength dependence. Ninety percent of the multiplexed light source was directed to the sample arm and the remaining ten percent was sent

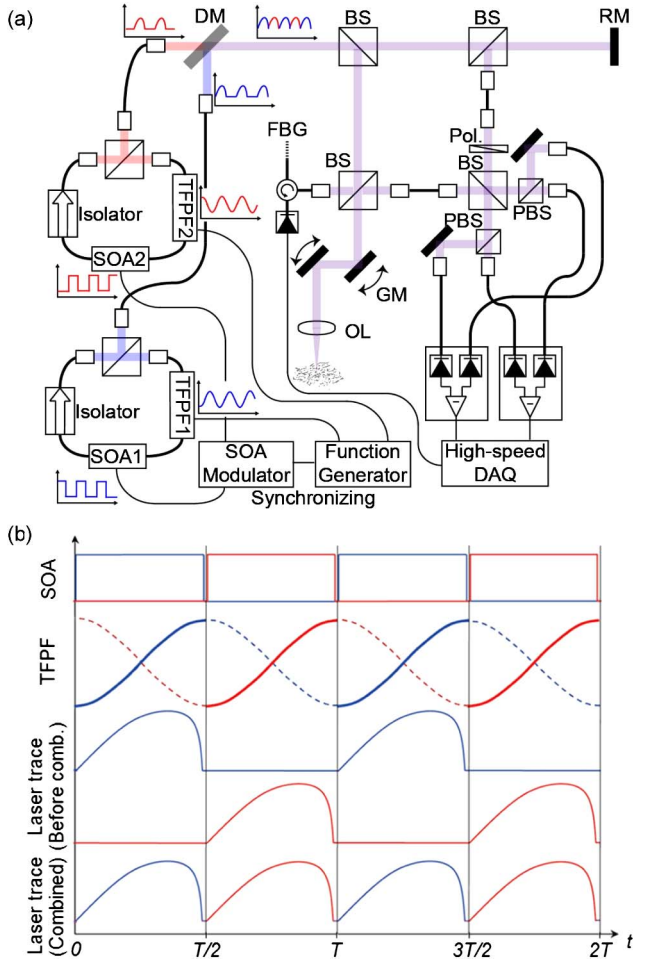

Fig. 1. (a) Schematic diagram of the dual-wavelength band OFDI system and (b) an illustration of laser modulation at each wavelength. Two short cavity wavelength swept laser sources with wavelength bands at 1040 nm (blue) and 1300 nm (red) were combined with a dichroic mirror. To minimize the wavelength dependence, a free-space optic system interferometer was built. SOA, semiconductor optical amplifier; TFPF, tunable Fabry–Perot filter; DM, dichroic mirror; BS, beam splitter; RM, reference mirror; FBG, Fiber Bragg grating; PBS, polarization beam splitter; GM, galvanometric mirror scanner; OL, objective lens.

to the reference arm. Half of the sample arm light was then delivered to the sample and another half was utilized for trigger signal generation. The sample arm light and the reference arm light were combined at the polarization-diverse, balanced detection setup, thereby generating the OFDI interference signal. A high-speed digitizer board (Signatec PX14400A) was used for fast acquisition of the signal. After acquisition, odd and even A-lines were separated, and each set of A-line generated images were acquired at 1.04 and 1.3 μm, respectively.

For exogenous contrast agents that could generate elastic resonant scattering in the 1040 and 1300 nm range, we custom-fabricated MNPs. Spherical MNPs are not the right choice for plasmon resonance in the near infrared (NIR) range. They are usually used in the visible region. Although we can push the resonance to longer wavelengths by increasing the size of the spherical MNPs, the resonant bandwidth becomes too broad and both strength and contrast of the resonance become very weak. On the other hand, the plasmon-resonant wavelength of the nonspherical MNP, which strongly depends on its geometry, is approximately proportional to the aspect ratio of the particle [8]. The resonance wavelength of nonspherical MNPs such as gold nanorods and triangular silver nanoplates can therefore reach to the 1.3 μm region as we increase the aspect ratio. We also required stronger scattering rather than absorption. When we illuminate MNPs with their resonant wavelength, both absorption and scattering occur. In the case of spherical MNPs, the size dependence on the scattering and the absorption cross sections can be given by

$$C_{\text{sca}} = \frac{k^4}{6\pi}|\alpha|^2 = \frac{8\pi}{3}k^4a^6\left|\frac{\varepsilon-\varepsilon_m}{\varepsilon+2\varepsilon_m}\right|^2$$

$$C_{\text{abs}} = k\cdot\text{Im}[\alpha] = 4\pi k a^3\cdot\text{Im}\left[\frac{\varepsilon-\varepsilon_m}{\varepsilon+2\varepsilon_m}\right],$$

where k is the wavenumber, α is the polarizability, a is the radius, ε is the dielectric function of the nanoparticle, and ε_m is the dielectric constant of the surrounding medium [9]. The scattering cross section scales with the radius to the sixth, whereas the absorption cross section scales with the radius to the third. In other words, we needed to use relatively large-sized particles in order to achieve stronger scattering than absorption at resonance. Therefore, we custom-fabricated gold nanorods with an average diameter of 8 nm and a length of 47 nm for resonant scattering in 1040 nm wavelength region. Additionally, we custom-fabricated triangular silver nanoplates with an average thickness of 20 nm and an edge length of 170 nm for resonant scattering in the 1300 nm region.

Figure 2 shows the normalized extinction spectrum of each type of nanoparticle that was measured. While the gold nanorods showed good resonance around the 1.0 μm wavelength, triangular silver nanoplates showed very broad and relatively weak resonance in the 1.3 μm wavelength region. The weak resonance was attributed to several causes including inhomogeneity of the particle size. In order to demonstrate the validity of the nanoparticles as contrast agents in the dual-band spectroscopic OFDI system, we imaged nanoparticle solutions in a pair of adjacent plastic tubes embedded in a scattering phantom as shown in Fig. 3(a). The concentrations of both

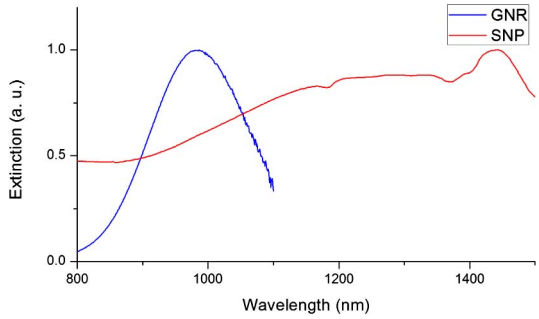

Fig. 2. Normalized extinction spectra of the gold nanorods (GNR) and the silver nanoplates (SNP) measured by a UV–Vis spectrometer. The gold nanorods and silver nanoplates were designed to have plasmon resonance at 1.0 and 1.3 μm, respectively.

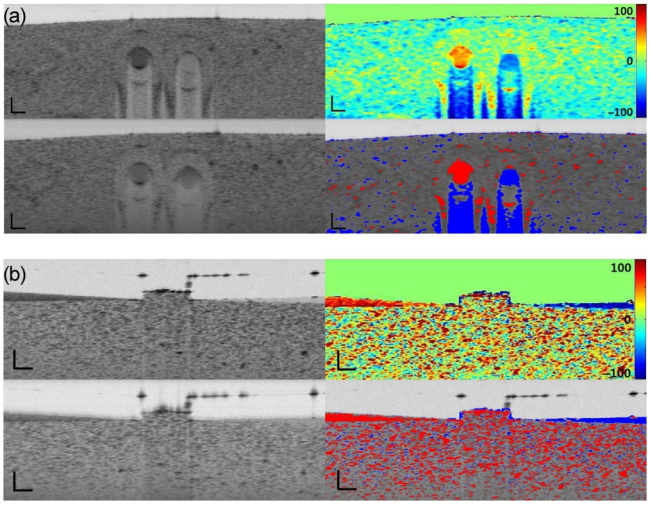

Fig. 3. Images of the nanoparticle solutions injected inside (a) two adjacent tubes and (b) gaps between scattering phantom and slightly inclined coverslips. The intensity images were normalized and median-filtered. For each set of images, (upper left) intensity image acquired with the 1.3 μm source, (lower left) intensity image acquired with the 1.0 μm source, (upper right) spectroscopic contrast image obtained by subtracting two intensity images, and (lower right) thresholded contrast superposed with the intensity image. The 1.3 μm resonant SNP is in the left tube (wedge) and the 1.0 μm resonant GNR is in the right tube (wedge). Scale bar: 100 μm.

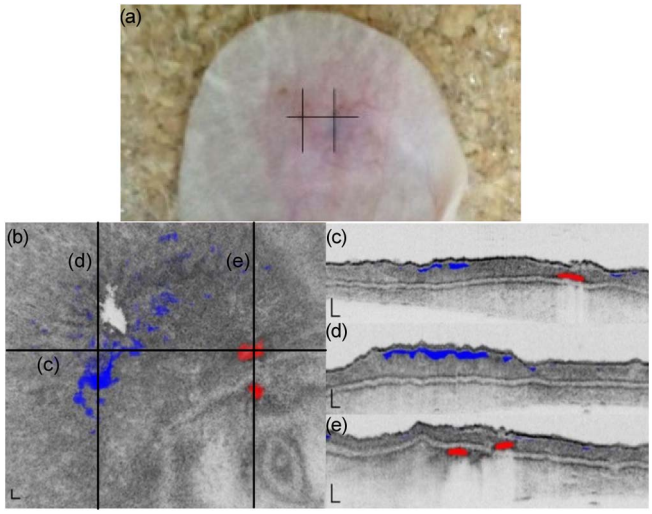

Fig. 4. (a) Photograph of a mouse ear after intradermal injection of the nanoparticle solutions. Thresholded contrast superposed with the intensity image (b) *en face*, (c) at the xz cross section, and (d), (e) at the yz cross section. The positions of xz and yz cross sections are indicated on the *en face* image. Red color represents 1.3 μm resonant silver nanoplates and blue color represents 1.0 μm resonant gold nanorods. Scale bar: 100 μm.

nanoparticles were 200 ppm, which corresponds to 7.4 nanomolar for gold nanorods and 93 picomolar for silver nanoplates. From the intensity images, 1.0 μm resonant gold nanorods showed a much stronger scattering signal when imaged with the 1.04 μm light source than with the 1.3 μm source, as expected. While 1.3 μm resonant silver nanoplates showed slightly stronger scattering in the images acquired with the 1.3 μm source compared to the 1.04 μm source, signal contrast between images of the nanoplates acquired with the resonant and nonresonant wavelengths was not as strong as the contrast obtained with 1.0 μm nanorods. We attribute this to the relatively weak resonance of the silver nanoplates as was previously mentioned in Fig. 2. To visualize the location of each nanoparticle in the sample more effectively, we generated a color-coded contrast image. We first compensated signal decay over depth by using the average intensity at each depth position from the surface of the sample. The intensity levels of a pair of images obtained at 1.04 and 1.3 μm were then normalized. The contrast image was finally obtained by subtracting these intensity images pixel by pixel after applying a 5 by 5 median filter, as shown in the upper right side of Fig. 3(a). The nanoplates appeared red (positive) while the nanorods appeared blue (negative). The color-coded image with proper thresholding was superposed with the intensity image showing good registration of each nanoparticle in the sample, as shown in the lower right side of Fig. 3(a). Since a spectroscopic OFDI image was obtained from a pair of intensity images acquired using the full wavelength tuning ranges of the two WSLs, it did not suffer from degradation of axial resolution compared with the corresponding intensity image. To show this, we imaged the nanoparticle solutions injected between the scattering phantom and the slightly inclined glass coverslip, which displayed a wedge shaped formation of nanoparticle solutions. The concentration of the gold nanorods was 200 ppm and the concentration of the silver nanoplates was 300 ppm (140 picomolar). The color-coded image obtained with 3 by 3 median filtering [right side of Fig. 3(b)] was capable of distinguishing the nanoparticle solutions even at the sharp tip of the wedge, thereby demonstrating spectroscopic OFDI imaging with high axial resolution. For *in vivo* imaging, we imaged a mouse ear following intradermal injection of the same nanoparticle solutions. The concentration of the gold nanorods was 0.9 mg/ml and the concentration of the silver nanoplates was 0.5 mg/ml. Although nanoparticles tended to diffuse rapidly in the tissue, especially the gold nanorods, both nanoparticles were successfully detected and distinguished, as shown in Fig. 4.

In summary, we have demonstrated a novel dual-wavelength band OFDI system that provides high-resolution spectroscopic imaging with MNPs as exogenous contrast agents. Utilizing a local increase of the OFDI signal by elastic plasmon-resonant scattering from two different custom-fabricated nonspherical MNPs with resonant wavelengths matching each wavelength band of the system, we were able to detect and distinguish each of the MNPs in a scattering phantom and in biological tissue. Designing and fabricating MNPs with better resonance characteristics, especially at the 1300 nm region, and expanding to other wavelength bands will further increase the potential and utility of this scheme.

This research was supported in part by the NRF of Korea, grant 2010-0017465, and by the MSIP of Korea, grants GFP/(CISS-2012M3A6A6054200) and NIPA-2013-H0401-13-1007.

References

1. U. Morgner, W. Drexler, F. X. Kärtner, X. D. Li, C. Pitris, E. P. Ippen, and J. G. Fujimoto, Opt. Lett. **25**, 111 (2000).
2. F. E. Robles, C. Wilson, G. Grant, and A. Wax, Nat. Photonics **5**, 744 (2011).
3. A. L. Oldenburg, M. N. Hansen, T. S. Ralston, A. Wei, and S. A. Boppart, J. Mater. Chem. **19**, 6407 (2009).
4. Y. L. Li, K. Seekell, H. Yuan, F. E. Robles, and A. Wax, J. Biomed. Opt. **3**, 1914 (2012).
5. S. H. Yun, G. J. Tearney, J. F. de Boer, N. Iftimia, and B. E. Bouma, Opt. Express **11**, 2953 (2003).
6. M. A. Choma, M. V. Sarunic, C. Yang, and J. A. Izatt, Opt. Express **11**, 2183 (2003).
7. H. S. Cho, S. J. Jang, K. Kim, A. V. Dan-Chin-Yu, M. Shishkov, B. E. Bouma, and W. Y. Oh, Biomed. Opt. Express **5**, 223 (2014).
8. S. Link, M. B. Mohammed, and M. A. El-Sayed, J. Phys. Chem. **103**, 3073 (1999).
9. S. A. Maier, in *Plasmonics: Fundamentals and Applications* (Springer, 2007), p. 65.